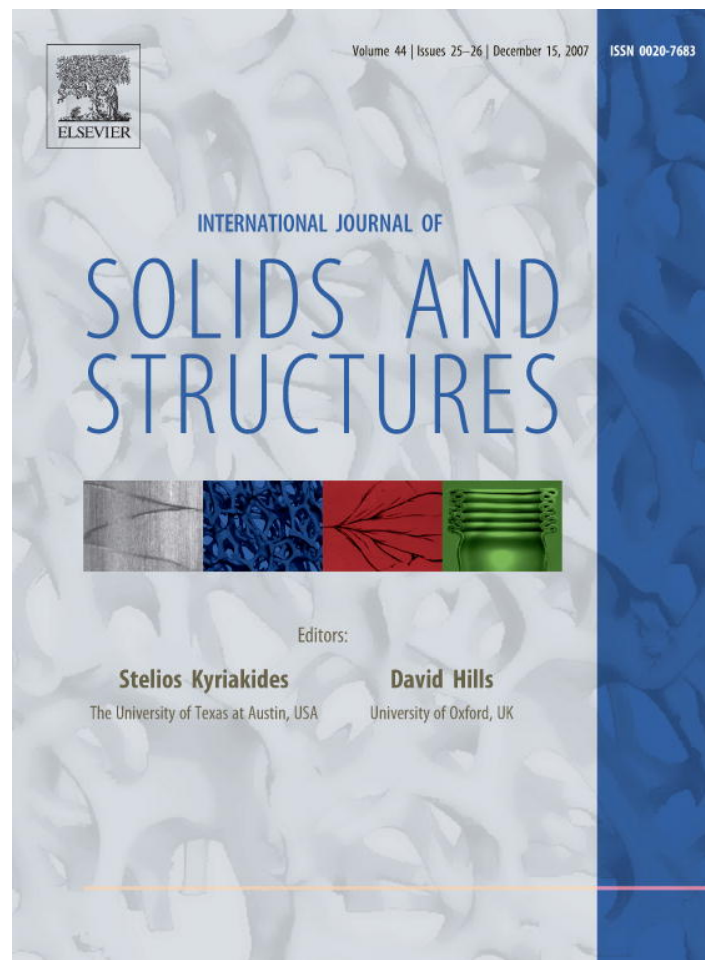


Provided for non-commercial research and education use.  
Not for reproduction, distribution or commercial use.



This article was published in an Elsevier journal. The attached copy is furnished to the author for non-commercial research and education use, including for instruction at the author's institution, sharing with colleagues and providing to institution administration.

Other uses, including reproduction and distribution, or selling or licensing copies, or posting to personal, institutional or third party websites are prohibited.

In most cases authors are permitted to post their version of the article (e.g. in Word or Tex form) to their personal website or institutional repository. Authors requiring further information regarding Elsevier's archiving and manuscript policies are encouraged to visit:

<http://www.elsevier.com/copyright>



# On the role of varying normal load and of randomly distributed relative velocities in the wavelength selection process of wear-pattern generation

N.P. Hoffmann <sup>\*</sup>, M. Misol

*Mechanics and Ocean Engineering, Hamburg University of Technology, Eißendorfer Straße 42, 21073 Hamburg, Germany*

Received 15 January 2007; received in revised form 25 May 2007; accepted 4 July 2007

Available online 24 August 2007

---

## Abstract

In systems with moving contacts, as e.g. automotive vehicles on dirt-roads, friction brakes, and of course railway vehicles moving on railway tracks, spatially periodic wear patterns may appear on the contact partners' surfaces. There is general agreement that the patterns are related to structural resonances. Using simple models with a moving point contact and an idealized wear model the present work first reviews some of the present understanding of wear-pattern generation. Then additional intuitively accessible explanations for the phenomena observed are developed and the effect of randomly specified relative velocities on the wavelength selection process is investigated. For this purpose the stability analysis of the surface evolution equation is pursued with the full, as well as with a reduced system, and a simple linear approach to deal with distributions of relative velocities is introduced. For fixed relative velocity the analysis yields an intuitively accessible picture of wear-pattern appearance or evanescence, as well as of wear-pattern motion. Based on these results it is shown, how dominant wavelengths are selected as a consequence of randomly distributed relative velocities.

© 2007 Elsevier Ltd. All rights reserved.

*Keywords:* Vibration; Wear pattern; Pattern formation; Stability

---

## 1. Introduction

Many engineering systems comprise some sort of moving contact, e.g. in ground vehicles the tyre-road or wheel-track contact point moves along the road or rail, in disk brakes the brake pad moves relatively to the turning brake disk, in cutting machines tools move along a work-piece, etc. All of these systems may show the emergence of wear patterns. Dirt roads, for example, may evolve into 'washboards', confer to Kurtze et al. (2001), where washboard-forming processes are investigated, and to Both et al. (2001) where also dissipative mechanisms related to the road surface (due to rain, etc.) are taken into account. Then of course there is the phenomenon of rail corrugation, which has been observed and studied already in the 19th century: train track

---

<sup>\*</sup> Corresponding author. Tel.: +49 (0) 40 42878 3120; fax: +49 (0) 40 42878 2028.  
E-mail address: [norbert.hoffmann@tuhh.de](mailto:norbert.hoffmann@tuhh.de) (N.P. Hoffmann).

as well as train wheels often show strikingly periodic changes in topography. The literature on the field is tremendous, and the quest for solving or at least dealing satisfactorily with the effect may still not be considered as concluded. Instead of attempting to give an overview about the many facets of the field, we refer to the recent reviews by Grassie and Edwards (2006), Meehan et al. (2005), Nielsen et al. (2003), Sato et al. (2002), Grassie and Kalousek (1993). But also disks of disk brakes may develop substantial thickness variations during operation (e.g. Schumann and Winner, 2006), which was the original motivation for the present work. In all of these cases the wear patterns generated usually lead to unwanted consequences, as e.g. vibrations, noise or structural damage.

A number of fundamental mechanisms have been proposed for explaining the appearance of the wear patterns. Among those in the following we will consider only the mechanisms which explain the appearance of wear patterns from homogeneous initial conditions, by this focussing on what often is called the pattern-formation aspect. In this class, two categories may be distinguished: first, for systems generating substantial changes in surface temperature due to frictional heating, thermoelastic instabilities may generate a change in the surface topography that again will interact with the wear mechanisms (Afferante et al., 2006, Steffen, 1998). Second, when temperature changes are of minor importance, the origin of the wear patterns is usually attributed to the existence of structural resonances that leave their footprints on the interface, such that wear patterns with spatial wavelengths correlated with the structural resonance frequencies and the velocity of relative motion appear. The present work focusses on systems of this second kind, not related to temperature effects.

The general picture of the interaction of structural vibration modes and spatially inhomogeneous wear has now been confirmed by a large number of full-scale numerical simulations, predominantly based on time-integrations, cf. e.g. to Meehan et al. (2005), Frischmuth and Langemann (2003), Küsel and Brommundt (2003), Meinders and Meinke (2003), Meywerk and Brommundt (2000), Brommundt (1997), Meywerk and Brommundt (1997). The main difficulty of these approaches might be considered to originate in the discrepancy between the time-scales of the – comparatively fast – structural oscillations and the – comparatively slow – time-scales of the wear processes. This may lead to a large computational effort, sometimes making it difficult to determine boundaries of critical parameter regimes, or to perform optimization approaches.

Consequently, in parallel to full-scale numerical approaches, a fruitful line of research into simplified or reduced-order modeling and analysis has developed. The work in this field either aims at gaining improved understanding of the fundamental mechanisms of the wear patterns' generation processes (Müller, 2001), or at developing more efficient computational approaches (e.g. Meehan et al., 2005). Instead of relying on time-integration, most of the approaches in this field consider wear pattern generation as an instability phenomenon: structural resonances lead, due to temporal variations of contact properties, to spatially inhomogeneous wear resulting in a surface-topography variation, that in turn may excite the structural dynamics. It is this feedback-loop that is generally thought to generate the surface wear patterns.

Since the structural resonance frequencies are typically largely unaffected by the relative velocity between the contact partners, the above reasoning would directly lead to the conclusion that – other parameters held constant – the wavelength of the wear patterns should be proportional to the relative velocity. It seems however, that there is still some debate if this result corresponds to what is observed in the field. E.g. in rail corrugation studies a number of field studies have not shown a clear linear relationship between train speed and corrugation wavelength (e.g. Bhaskar et al., 1997). In contrast, the idea that the corrugation wavelength could be independent of the train speed, exists.

The present work addresses this question of wavelength selection by considering constant and randomly distributed relative velocities. Remarkably, only very recently work on the effects of non-constant relative velocities seems to have been undertaken. To the authors' knowledge Bellette et al. (2006) seem to have been the first investigators to analyze varying train speeds in the context of a frequency-domain stability analysis. They find substantially reduced growth rates when the train speed is not the same for all trains, but statistically distributed around a mean value. An evaluation of the effects of non-constant relative velocities on wavelength selection and wear-pattern motion however seems still to be missing. The present work therefore investigates the effect of randomly distributed relative velocities on wear-pattern formation.

The paper is structured as follows: first a single-degree-of-freedom model is introduced. The full and the linearized evolution equations are derived and the stability of the surface subjected to wear for a given con-

stant relative velocity is investigated from the full system, as well as from a reduced system obtained by an averaging approach. In addition to this quantitative mathematical analysis an intuitively accessible approach to understanding the instability's appearance is presented. The approach is then extended to an exemplary two-degree-of-freedom structural system. Subsequently exemplary velocity distributions are considered and an extended linear analysis for dealing with such load cases is presented and evaluated. Finally an outlook is given that addresses questions of extending the approach presented to aspects not considered yet.

## 2. A review on the mechanism of wear-pattern generation by normal force variation

### 2.1. A single-degree-of-freedom model and its evolution equations

Probably the most generic model to study the interaction between structural oscillations and wear-pattern generation may be taken as a single-degree-of-freedom linear harmonic oscillator moving with a constant horizontal speed  $V$  over an originally plane surface, which experiences wear due to the relative motion of the moving oscillator. For the analytical approach we closely follow Kurtze et al. (2001) to simplify comparison of the subsequently extended modeling and analysis with the previously available work. A sketch of the system is given in Fig. 1.

The mass of the oscillator is denoted by  $m$  and it is assumed to be coupled to the surface through a linear spring with spring stiffness  $k$  and a linear viscous damping element of damping constant  $d$ . With  $Z(x)$  denoting the vertical position of the mass and  $H(x)$  denoting the height of the counter-surface at the momentary position  $x$  of the mass, the evolution equation for the structural oscillation of the mass at its current position reads

$$m \frac{D^2}{Dt^2} Z + d \frac{D}{Dt} (Z - H) + k(Z - H) = 0, \quad (1)$$

where  $D/Dt$  stands for the derivative evaluated at the momentary position of the mass – i.e. the ‘material derivative’. To simplify the analysis the equation is now divided by  $m$  and a natural undamped (angular) frequency  $\omega_0 = \sqrt{k/m}$  as well as a damping parameter  $\Gamma = d/(m\omega_0)$  are introduced. The next step is to connect the model of the discrete moving mass, described by the ordinary differential equation given above, with a model describing the wear of the counter-surface. For that purpose the model of the moving discrete oscillator is now replaced by an ensemble of moving oscillators, such that the ordinary differential Eq. (1) can be replaced by a partial differential equation that may subsequently be coupled to a wear evolution equation of the counter-surface to be specified later. Formally this extension is accomplished by evaluating the material derivative  $D/Dt$  as  $D/Dt = \frac{\partial}{\partial t} + V \frac{\partial}{\partial x}$ , where  $V$  stands for the (advection) velocity of the oscillator relative to the surface. By this substitution the Lagrangian coordinate representation is converted into a Eulerian representation and the resulting evolution equation reads

$$(\partial_t + V\partial_x)^2 Z(x, t) + \Gamma\omega_0(\partial_t + V\partial_x)(Z(x, t) - H(x, t)) + \omega_0^2(Z(x, t) - H(x, t)) = 0. \quad (2)$$

For the wear model we assume proportionality of the amount of wear with the normal load exerted by the moving oscillator, i.e. an Archard type wear model. Of course this is a highly simplified approach, compare e.g. Nielsen et al. (2003) for models based on more physical insight into the specific wear processes of rail corrugation. For the purpose of the present work, which was motivated primarily by corrugation in brake disks,

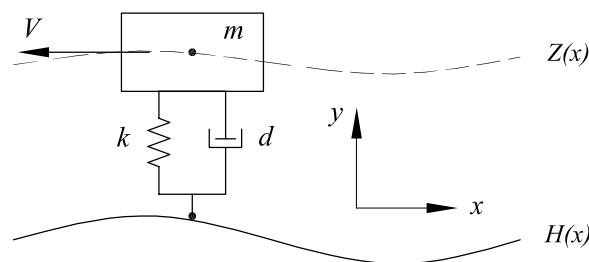


Fig. 1. Single-degree-of-freedom system.

this simplification however seems adequate: first, Archard's wear law is very widespread in evaluating wear in braking systems, second, the work is to show a basic approach rather than a detailed tribological representation of the certainly manifold wear processes, which are definitely specific to the selected application. It should however be possible to adapt the techniques presented in the following also to alternative wear models and derive corresponding results.

With  $m[g + (\partial_t + V\partial_x)^2 Z]$  being the normal load onto the surface, the surface evolution equation simply reads

$$\partial_t H(x, t) = -ma(H)[g + (\partial_t + V\partial_x)^2 Z(x, t)], \quad (3)$$

where an additional factor  $a(H)$  parameterizing the wear rate as a function of the surface height has been introduced to allow for a dependency of the wear rate on the state of the surface topography.

Eqs. (2) and (3) form a coupled set of partial differential equations describing both the dynamics of the oscillator in motion as well as the wear evolution of the counter-surface. To simplify the analysis, the fields are now decomposed into a component corresponding to a spatial mean value, depending on time only, and into the deviation from that mean, i.e.  $H$  and  $Z$  are decomposed into

$$H(x, t) = H_0(t) + h(x, t), \quad Z(x, t) = Z_0(t) + z(x, t), \quad (4)$$

where  $h$  and  $z$  are assumed to have a vanishing spatial average. In addition the wear equation – as the only nonlinear-equation under consideration – is linearized with respect to the spatially dependent variables, since for the purpose of the present work we are merely interested in the stability of a spatially homogeneous wear evolution around the spatially averaged surface height  $H_0$ . After linearizing Eq. (3) and subtracting the spatially averaged equations to obtain equations for  $h$  and  $z$ , the result is

$$\begin{aligned} \partial_t H_0 &= -ma(H_0)[g + \partial_u^2 Z_0], \\ \partial_t h &= -m \frac{\partial a}{\partial H} \Big|_{H_0} h(g + \partial_u Z_0) - ma(H_0)(\partial_t + V\partial_x)^2 z, \end{aligned} \quad (5)$$

$$\begin{aligned} \partial_u^2 Z_0 + \Gamma\omega_0\partial_t(Z_0 - H_0) + \omega_0^2(Z_0 - H_0) &= 0, \\ (\partial_t + V\partial_x)^2 z + \Gamma\omega_0(\partial_t + V\partial_x)(z - h) + \omega_0^2(z - h) &= 0. \end{aligned} \quad (6)$$

Note that the evolution equations for the spatially averaged quantities are decoupled from the evolution of the spatially dependent variables. This means that the averaged wear level will proceed irrespective of any spatially inhomogeneous wear dynamics.

To obtain solutions for the equations determining the spatial inhomogeneities, two approaches may be followed. First, solutions for the coupled system of structural and wear dynamics can be obtained. For that purpose it seems plausible to assume that the quantities  $a(H_0)$  and  $\frac{\partial a}{\partial H} \Big|_{H_0}$  – through their implicit time-dependency – vary only very slowly with time, and can therefore be approximated by constants. In addition the term  $m \frac{\partial a}{\partial H} \Big|_{H_0} h \partial_u Z_0$  is neglected, since – in the spirit of setting slowly varying variables constant – it would basically result in a slowly time-dependent rescaling of the constant  $g$ .

Then the resulting equations for  $h$  and  $z$  are temporally and spatially homogeneous and solutions can be sought in the form  $h(x, t) = \hat{h} \exp(ikx + st)$ ,  $z(x, t) = \hat{z} \exp(ikx + st)$ , where  $k$  is the wavenumber (which is  $2\pi$  times the inverse of wavelength),  $\text{Re}(s)$  the growth rate and  $\text{Im}(s)$  the corresponding frequency. The approach reduces the set of partial differential equations to the homogeneous set of algebraic equations

$$\begin{bmatrix} s + m g \frac{\partial a}{\partial H} \Big|_{H_0} & ma(H_0)(s + ikV)^2 \\ -\Gamma\omega_0(s + ikV) - \omega_0^2 & (s + ikV)^2 + \Gamma\omega_0(s + ikV) + \omega_0^2 \end{bmatrix} \cdot \begin{pmatrix} \hat{h} \\ \hat{z} \end{pmatrix} = 0. \quad (7)$$

Solvability requires the determinant of the coefficient matrix to vanish, such that by evaluating the resulting third order polynomial in  $s$  a dispersion relation with three roots can be deduced.

Although the approach is straightforward, in more general cases than the one considered here the calculation strategy may run into difficulties, since in fact the resulting eigenvalues capture the fast vibrational dynamics as well as the slow wear evolution. The large differences in the absolute values of the corresponding eigenvalues may therefore result in extremely stiff equations, possibly hard to solve. To overcome this problem

one may derive a reduced-order equation for the wear-pattern evolution by following an averaging strategy. Assuming that from the fast structural vibration only the pressure obtained from averaging over the fast vibration time-scale enters into the wear dynamics, all time derivatives acting on  $z$  may be eliminated. With this assumption the second part of Eq. (6) reduces to

$$(V\partial_x)^2 z + \Gamma\omega_0 V\partial_x(z - h) + \omega_0^2(z - h) = 0, \tag{8}$$

which – assuming the exponential ansatz already introduced – may be solved for  $z$  as a function of  $h$ , i.e.

$$z = [\omega_0^2 - V^2k^2 + ik\Gamma\omega_0 V]^{-1}(\omega_0^2 + ik\Gamma\omega_0 V)h. \tag{9}$$

In turn this relation may then be introduced into Eq. (5) to obtain – neglecting in addition the temporal change of  $\partial_t z$  relative to its spatial variation  $V\partial_x z$  – an explicit evolution equation for the height  $h$  only:

$$\partial_t h = -\beta h - ma(H_0) \left[ \frac{(\omega_0^2 + ik\Gamma\omega_0 V)}{\omega_0^2 - V^2k^2 + ik\Gamma\omega_0 V} \right] (-V^2k^2)h. \tag{10}$$

Here a nonlinearity parameter  $\beta = mg \frac{\partial a}{\partial H} |_{H_0}$  has been introduced for abbreviation. The corresponding dispersion relation can correspondingly be stated in explicit form as

$$s = -\beta + ma(H_0)V^2k^2 \left[ \frac{(\omega_0^2 + ik\Gamma\omega_0 V)}{\omega_0^2 - V^2k^2 + ik\Gamma\omega_0 V} \right]. \tag{11}$$

With this all the required algebra is provided to evaluate the wear-pattern evolution for the case of constant relative velocity, as well as for the case of a superposition of relative velocities. This is pursued in the subsequent sections.

### 2.2. Results from the averaging approach

To show the fundamental phenomena occurring in the system, especially also with a view to the subsequent investigation of corrugation for varying relative velocities, we will restrain the analysis to the parameters  $m = 1$  kg,  $\omega_0 = 1/s$ ,  $a_0 = a(H_0) = 10^{-10}$  s kg<sup>-1</sup> and  $V = 1$  m/s. We will vary only the system's damping  $\Gamma$  and the parameter  $\beta$  characterizing the nonlinearity in the wear evolution equation. Fig. 2 shows the real part of  $s$ , i.e. the growth rate, and the corresponding imaginary part characterizing the translation of the wear pattern over time, vs. the wavenumber  $k$  for a number of different damping values and  $\beta = 0$ .

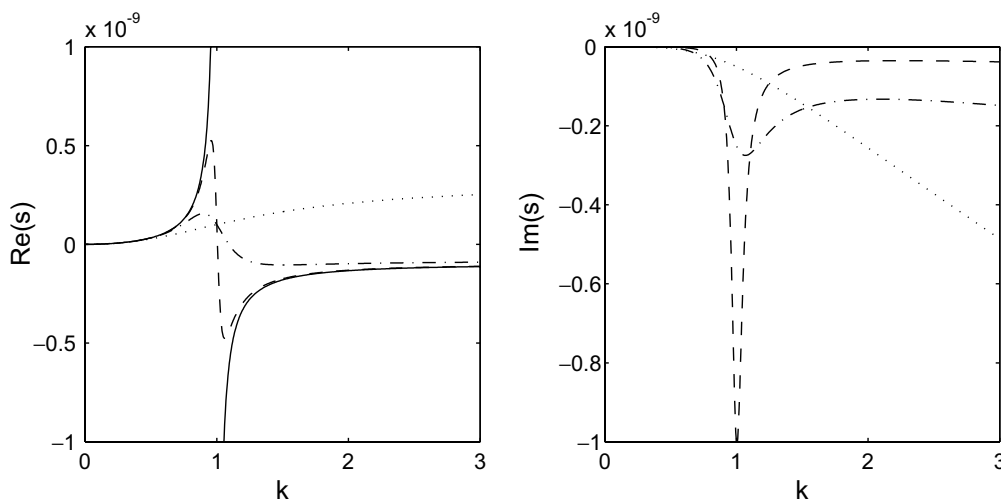


Fig. 2. Stability properties of the wear evolution equation for  $m = 1$  kg,  $\omega_0 = 1$  s<sup>-1</sup>,  $a_0 = a(H_0) = 10^{-10}$  s kg<sup>-1</sup>,  $V = 1$  m/s and  $\beta = 0$ .  $\text{Re}(s)$ , i.e. the growth rate (left), and  $\text{Im}(s)$ , i.e. the wear-pattern oscillation frequency (right) vs. the wavenumber  $k$  for  $\Gamma = 0$  (solid), 0.1 (dashed), 0.4 (dash-dotted) and 2.0 (dotted).

A number of results can be extracted from the analysis. Although some of the findings have already been obtained earlier using alternative modeling strategies (cf. e.g. Meehan and Daniel, 2006, Meehan et al., 2005, Kurtze et al., 2001), a review and overview seems appropriate. One may note: (1) For zero damping the dispersion relation is discontinuous: there is a wavenumber  $\tilde{k}$ , corresponding to resonant excitation of the oscillator ( $\tilde{k} = \omega_0/V$ ), such that all perturbations with wavenumbers below  $\tilde{k}$  are unstable, and when  $k$  approaches  $\tilde{k}$  from below, the growth rate diverges. In contrast, all perturbations with wavenumbers larger than  $\tilde{k}$  lead to stable configurations. (2) When the damping is weak, the dispersion relation becomes continuous, but still there is a maximum for the growth rates around  $\tilde{k}$ , whereas larger wavenumbers are again stable and asymptotically (for  $k \rightarrow \infty$ ), a negative growth rate results. (3) For stronger damping (note that  $\Gamma = 2$  as chosen in the example corresponds to critical damping, i.e. Lehr's damping equal to 1), all wavenumbers yield instability, with larger wavenumbers being increasingly more unstable than smaller ones and the growth rate reaches a positive asymptotic limit for  $k \rightarrow \infty$ .

The whole situation changes only slightly when a dependency of the wear rate on the surface level is admitted, i.e. when non-zero  $\beta$  is considered. The explicit form for  $s$  directly shows that a non-zero, positive  $\beta$  merely leads to a decrease of the growth rate by a constant term. As a result, for weak damping the wavenumber range of instability will turn out as a bounded wavenumber interval, whereas for strong damping either all wavenumbers beyond a certain threshold, or no wavenumber at all will yield instability.

### 2.3. The intuitive picture

After the reduced-order model has been evaluated and discussed in a rather formal manner the question of course appears if the instabilities arising can also be understood from a simpler, more physics- or mechanism-oriented point of view. Although parts of the explanations presented have been given in a number of scattered publications, it seems worth while to attempt a reviewing description allowing for a complete picture.

For that purpose, consider the undamped system. After a small harmonic surface corrugation has evolved, this will be felt by the oscillator as an external forcing with the angular frequency  $Vk$ . Basically, Eq. (9) gives a frequency response of  $z$  due to a harmonic 'input' in  $h$ , see Fig. 3. Whenever the forcing frequency  $Vk$  is smaller than the oscillator's resonance frequency  $\omega_0$ , the response will be strictly in phase with the excitation. This however means that, considering again the transfer relation (9) between  $h$  and  $z$ , that  $z$  will be positive and larger than  $h$  when the mass moves over the 'hill', whereas it will be negative and smaller (i.e. more negative) than  $h$  when it moves through the 'valley'. This in turn means nothing but that over the hill the contact load will be smaller than in the valley, which in turn directly leads to an increased wear in the valleys and an overall amplitude growth of the surface corrugation. Analogously, when the 'exciting wavenumber' is larger than  $\tilde{k}$ , the vibration response of the oscillator will have a phase shift of  $\pi$  with respect to the phase of the surface

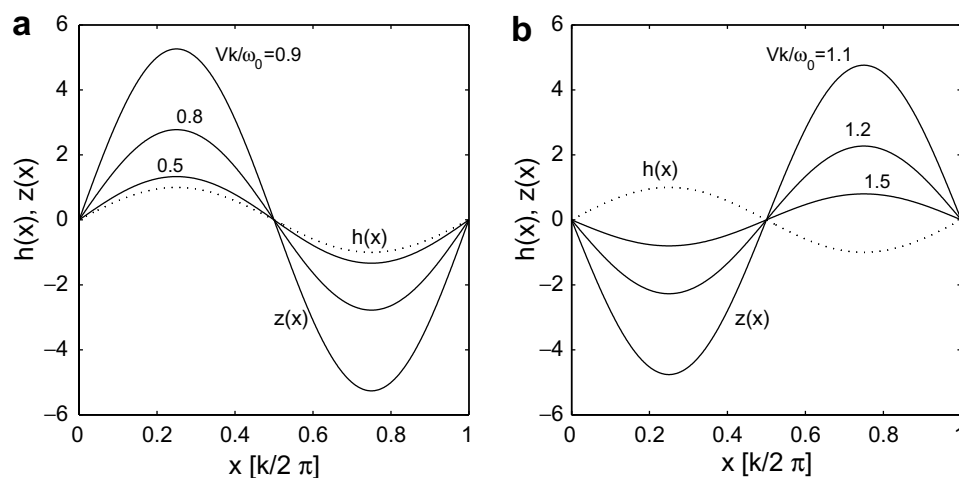


Fig. 3. Displacement  $z(x)$  of the undamped oscillator due to a harmonic surface corrugation  $h(x)$ . Excitation frequencies  $Vk$  below (a) and above (b) the oscillator's resonance frequency  $\omega_0$ .

corrugation, which means that the load is increased over the hills and decreased in the valleys, which will lead to the corrugation being wiped out. Moreover, the proximity of the forcing frequency  $Vk$  to the oscillator's resonance frequency  $\omega_0$  determines the strength of the process that either leads to a build-up of corrugation, or to its evanescence. The origin lies in the oscillator's resonance behavior, its amplitude and phase response due to a forcing from the surface corrugation, and thus convincingly explains the asymptotic stability behavior when  $Vk$  approaches  $\omega_0$ .

When the oscillator is damped, the transfer behavior of Eq. (9) will introduce spatial phase differences between the surface corrugation and the vertical displacement of the oscillator different from 0 or  $\pi$ . To understand the role of these phase differences better, in the following a phase shift of exactly  $\pi/2$  will be considered first, since an arbitrary phase lag may be decomposed into a component shifted by 0 or  $\pi$  (the 'in-phase-component') and a component shifted by  $\pi/2$  (the 'out-of-phase-component').

Fig. 4 shows a configuration in which there is a phase shift of exactly  $\pi/2$  between the surface-topography corrugation and the oscillator's pathway. This corresponds to the phase relation, when the oscillator, which moves towards the left, is resonantly excited through the surface corrugation. Repeating the reasoning with respect to wear it turns out that – for the configuration shown – the strongest wear results for the regions with the smallest elevations in  $z$ , whereas the weakest wear results where  $z$  is largest. Obviously, these areas correspond to the shoulder-areas in the corrugation topography: the upward-moving mass strongly wears the upward-shoulder, while the downward-moving mass yields reduced wear. With respect to overall stability these two effects balance; however, a differential wear between the upward and the downward shoulders of the surface corrugation will result in the corrugation pattern to move laterally. Following these arguments it is quite easy to understand that an out-of-phase relationship as depicted will lead to the oscillatory wear pattern moving towards the left, i.e. towards smaller  $x$ -values. Also, the larger the amplitude of the oscillator motion  $z$ , the stronger is the disparity in wear between the two shoulders, which corresponds to an increased differential wear, and by that to an increase in the lateral velocity of the wear pattern. Indeed, this result has already been obtained formally in the eigenvalue analysis of the preceding section, where the imaginary part  $\text{Im}(s)$  of the growth-rate attained a substantial value close to the oscillator's resonance frequency.  $\text{Im}(s)/k$  does however give nothing but the phase-velocity of the harmonic corrugations considered. Following the simple reasoning above, lateral motions of the wear patterns can thus also be well understood on the basis of the oscillator's dynamical response behavior.

In addition one may note that in the damped case the wavenumber corresponding to the most unstable perturbation no longer exactly coincides with the resonance frequency of the undamped structural system: damping reduces the frequency of maximum frequency response, and by that decreases the most critical wavenumber, cf. Fig. 2.

To summarize the results of this section: (1) the in-phase-component between a harmonic surface corrugation and the corrugation-induced vertical oscillation of the oscillator always results in an instability of the sur-

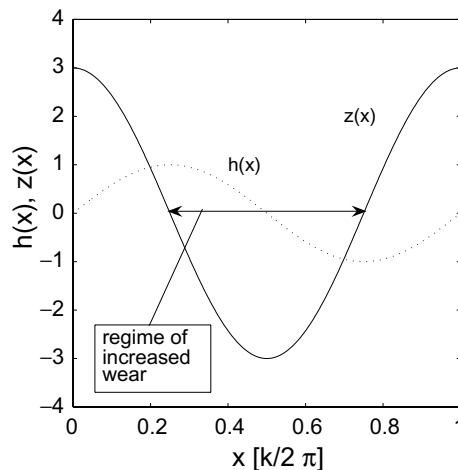


Fig. 4. Out-of-phase displacement  $z(x)$  due to a harmonic surface corrugation  $h(x)$ .

face evolution equation, related to an increase of the surface corrugation. (2) A phase shift of  $\pi/2$ , i.e. an out-of-phase-relation, with the oscillator ‘lagging behind’ the surface corrugation, results in a neutrally stable configuration, which is however linked to a lateral motion of the wear patterns. (3) Finally, a phase shift of  $\pi$  always leads to a reduction of the corrugation, such that the vibration dynamics wipes out the surface elevations.

From these considerations it becomes evident, why for strongly damped oscillators the surface evolution in the model always shows unstable behavior: for the strongly damped oscillator the phase lag between the exciting surface topography and the vertical position never exceeds  $\pi/2$ , but always remains in the interval  $[0, \pi/2]$ . Consequently, strongly damped oscillators will always render the counter-surface unstable with respect to corrugations.

It should be noted here that similar arguments have been applied also in the context of flow-induced ripple-formation in granular material (e.g. sand) under shear flows. It seems plausible that the underlying mechanisms of both processes should be largely analogous (compare e.g. [Charru and Hinch, 2006](#)) in mechanical terms.

#### 2.4. Comparison to solutions of the full system

Although the above approach to evaluate wear-pattern stability seems convincingly simple, and also an intuitive explanation for the resulting stability behavior is at hand, still there is some lack of confidence in the quality of the approximation method used. Without a doubt the approach is somewhat ‘handwaving’, which leaves one with some doubts about the question, if the behavior of the full system has in fact been reduced correctly. To evaluate these problems, the eigenvalue problem corresponding to the full system (7) is tackled in the following. Of course such a direct computation could be difficult in systems of larger size, but for the present conceptual model a direct comparison is possible. Among the most important questions to be answered is the sensitivity of the reduced-order approach with respect to the strength of the wear rate, since often in large-scale modeling – due to the too high computational effort in using wear rates of true size – a wear rate upscaling is used, tacitly assuming that the overall interplay between the structural and the wear dynamics will remain unchanged. Some limits of this approach will appear in the following.

[Fig. 5](#) shows  $\text{Re}(s)$  and  $\text{Im}(s)$  as calculated from the coupled system of Eq. (7) for the exemplary parameters already used for the averaging approach with a damping parameter of  $\Gamma = 0.1$ . Obviously, both structural modes as well as surface-topography modes are now recovered: the structural modes result in strongly negative real parts of the eigenvalues, due to the damping prescribed. In addition, a variation of the wavenumbers leads to constantly decreasing imaginary parts of their corresponding eigenvalues.

In contrast, the eigenvalues corresponding to the surface evolution have only very small values and cannot be resolved on the scales of the structural system’s eigenvalues. When magnified, the dependency of the surface evolution on the wavenumber however becomes marked. Interestingly, for the parameters chosen differences between the full system’s eigenvalues corresponding to a surface evolution and the eigenvalues resulting from the averaging approach are not visible to the bare eye, showing that the averaging approach in fact captures the significant parts of the dynamics.

At this point it is also rewarding to examine the influence of upscaling the wear rate parameter, which is often done in modeling and simulation approaches based on time-series evolution, since otherwise results cannot be obtained in a reasonable amount of computational time. [Fig. 6](#) shows the results of the full system’s eigenvalues for increasing wear rates.

For strongly increased wear rates the structural modes and the surface evolution modes can no longer be regarded as uncoupled modes. In the example considered first influences on the structural modes can be noticed for wear rates of the order of  $a(H_0) = 10^{-4} \text{s kg}^{-1}$ . At  $a(H_0) = 10^{-2} \text{s kg}^{-1}$  another effect results: the surface evolution mode couples strongly to the vibration modes for large wavenumbers, since the growth rates (i.e. the real parts of the eigenvalues) become comparable. At first sight these results might seem artificial, since growth rates for the surface evolution of this size are of course unphysical. However, there remains the fundamental problem that upscaling the wear rate may quantitatively change the spectral characteristics of the system; and this quantitative change may hardly be estimated a priori, as the small sample

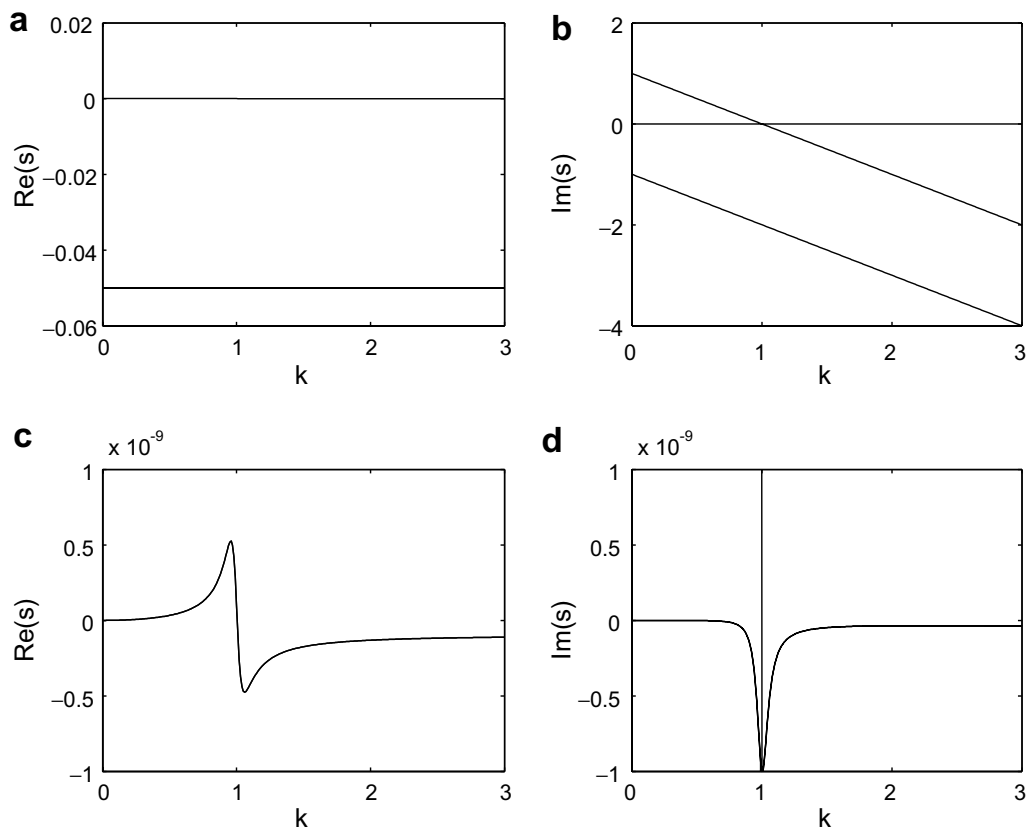


Fig. 5. Resulting eigenvalues from Eq. (7) for  $m = 1$  kg,  $\omega_0 = 1$  s $^{-1}$ ,  $a_0 = a(H_0) = 10^{-10}$  s kg $^{-1}$ ,  $V = 1$  m/s,  $\beta = 0.1$  s $^{-1}$  and  $\Gamma = 0.1$ . (a) and (b) show the full range, (c) and (d) give magnified views of the eigenvalues corresponding to surface evolution. In (c) and (d) the eigenvalues resulting from the averaging approach are also plotted, but cannot be distinguished from the corresponding eigenvalues of the full system.

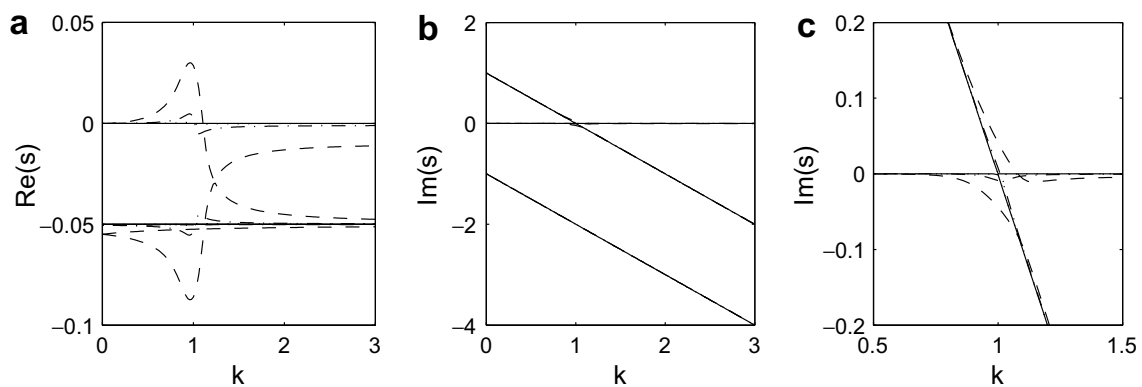


Fig. 6. Results of the eigenvalue analysis from Eq. (7) for  $m = 1$  kg,  $\omega_0 = 1$  s $^{-1}$ ,  $V = 1$  m/s,  $\beta = 0.0$ ,  $a_0 = a(H_0) = 10^{-10}$  (solid),  $10^{-4}$  (dotted),  $10^{-3}$  (dash-dotted),  $10^{-2}$  (dashed) s kg $^{-1}$ . (a) and (b) show the full range, (c) gives a magnified view of the imaginary components. It shows that for the largest wear rate the structural and the surface evolution modes have coupled.

calculation shows. Especially, the smaller the system's structural damping, the closer the growth rate of the surface evolution mode will be to the growth rates of the structural modes and the mutual interference might quickly limit upscaling wear rates. It might therefore be considered a valuable task for future studies to develop measures that would allow a priori, i.e. without performing first an eigenvalue analysis of the complete coupled system, an evaluation of the allowable amount of upscaling the wear rate in computational approaches.

### 3. Wear-pattern generation in a two-degree-of-freedom structural system

The preceding section focused on wear-pattern generation due to a single resonance in the structural system. It turned out that for weakly damped systems instability in the topography evolution will typically result for a wavenumber band with an upper limit close to the undamped system's resonance frequency. For over-damped systems instability may result for all wavenumbers larger than a critical value below the resonance frequency. Since real technical systems are usual characterized by a number of modes larger than one in the present section an exemplary two-degree-of-freedom structural model is investigated.

#### 3.1. The model and its evolution equations

The system, see Fig. 7, might be understood e.g. as a quarter car model moving with constant velocity over a road or as a brake pad sliding over a brake disk, where both the pad's lining stiffness, as well as the hydraulic system is taken into account.

Proceeding in complete analogy to the single-degree-of-freedom system, the equations determining the structural oscillations are

$$\begin{aligned} m_2 \frac{D^2}{Dt^2} Z_2 + d_2 \frac{D}{Dt} (Z_2 - Z_1) + k_2 (Z_2 - Z_1) &= 0, \\ m_1 \frac{D^2}{Dt^2} Z_1 + d_2 \frac{D}{Dt} (Z_1 - Z_2) + d_1 \frac{D}{Dt} (Z_1 - H) + k_2 (Z_1 - Z_2) + k_1 (Z_1 - H) &= 0, \end{aligned} \quad (12)$$

where  $H$  denotes the surface corrugation,  $Z_1$  and  $Z_2$  the vertical position of the masses  $m_1$  and  $m_2$ , and  $k_1$  and  $k_2$  and  $d_1$  and  $d_2$  denote the stiffness as well as the damping parameters, respectively.

From these equations the normal load exerted onto the surface can easily be identified as

$$N = (m_1 + m_2)g - d_1 \frac{D}{Dt} (Z_1 - H) - k_1 (Z_1 - H), \quad (13)$$

such that the surface evolution equations do result in

$$\partial_t H = -a(H)N. \quad (14)$$

Again all variables are decomposed into a spatially homogeneous and a spatially inhomogeneous part, for which a harmonic form is assumed, e.g.  $H(x, t) = H^0(t) + h(t)\exp(ikx)$ , etc. Since the structural system has already been assumed linear the corresponding equations are also the evolution equations for the spatially inhomogeneous quantities. The surface evolution equation has however to be linearized first and results in

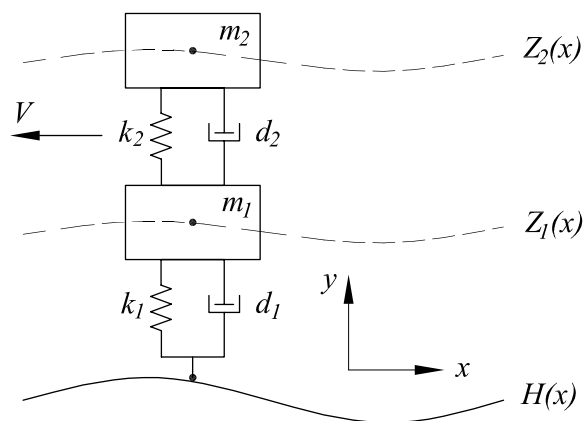


Fig. 7. Two-degree-of-freedom system.

$$\begin{aligned} \partial_t H^0 &= -a(H^0) \left[ mg - d_1 \frac{D}{Dt} (Z_1^0 - H^0) - k_1 (Z_1^0 - H^0) \right] \\ \partial_t h &= -\beta h + a(H^0) \left[ d_1 \frac{D}{Dt} (z_1 - h) + k_1 (z_1 - h) \right]. \end{aligned} \quad (15)$$

Since the resulting system is – assuming  $a(H^0)$  and  $\beta$  as approximately constant – again invariant with respect to time, an exponential time-dependency can be separated, writing  $h, z_1, z_2 \exp(st)$ , which allows to replace  $\frac{D}{Dt}$  by  $(s + ikV)$ . This yields a homogeneous algebraic system:

$$\begin{bmatrix} s + mg \frac{\partial a}{\partial H} \Big|_{H^0} & -a(H^0) d_1 (s + ikV) & 0 \\ +a(H^0) d_1 (s + ikV) & -a(H^0) k_1 & \\ +a(H^0) k_1 & & \\ -d_1 (s + ikV) & m_1 (s + ikV)^2 & -d_2 (s + ikV) \\ -k_1 & +(d_1 + d_2) (s + ikV) & -k_2 \\ & +(k_1 + k_2) & \\ 0 & -d_2 (s + ikV) & m_2 (s + ikV)^2 \\ & -k_2 & +d_2 (s + ikV) \\ & & +k_2 \end{bmatrix} \cdot \begin{pmatrix} \hat{h} \\ \hat{z}_1 \\ \hat{z}_2 \end{pmatrix} = 0. \quad (16)$$

The roots of the corresponding characteristic polynomial then lead to three modes: two for structural oscillations, one for the surface evolution.

Also here an averaging approach may be devised. By averaging out the time-dependent terms in the structural evolution equations, and after introducing harmonic ansatz functions, the following algebraic equations including  $h, z_1$  and  $z_2$  remain:

$$\begin{aligned} m_2 (ikV)^2 z_2 + d_2 (ikV) (z_2 - z_1) + k_2 (z_2 - z_1) &= 0, \\ m_1 (ikV)^2 z_1 + d_2 (ikV) (z_1 - z_2) + d_1 (ikV) (z_1 - h) + k_2 (z_1 - z_2) + k_1 (z_1 - h) &= 0. \end{aligned} \quad (17)$$

These equations may be used to express  $z_1$  explicitly in terms of  $h$  to eliminate  $z_1$  from the surface evolution equation such that finally an explicit dispersion relation can again be obtained.

### 3.2. Exemplary results

Fig. 8 shows typical results from an eigenvalue analysis of the two-degree-of-freedom system for arbitrary parameters. Again sharp peak-like structures appear for the modes associated to surface evolution near those wavenumbers where the structural oscillations are excited resonantly.

The multi-degree-of-freedom structural model does not seem to provide any new qualitative features beyond what has already been analyzed in the case of the single-degree-of-freedom model. We therefore conclude the present analysis. It should however be remarked that an extension of the approach presented to systems with a spatially extended contact and wear area seems to be the next step in developing understanding and modeling approaches. This task is however left to future studies.

## 4. Randomly distributed relative velocities

Above it has been shown that the wavelength of the wear patterns is correlated with structural resonance frequencies leading to oscillatory normal force. Since the wavelength of the pattern should then be proportional to the relative velocity, this reasoning does not directly lead to a preferred wavelength for the wear pattern when loading ensembles comprising distributions of relative sliding speeds are considered. The present section shows, how, in a linear approximation, the preferred wavelengths, corresponding growth rates and propagation speeds of wear patterns can be determined in systems, for which the relative velocity between the contact partners is not constant, but can be given only in terms of a probabilistic description.

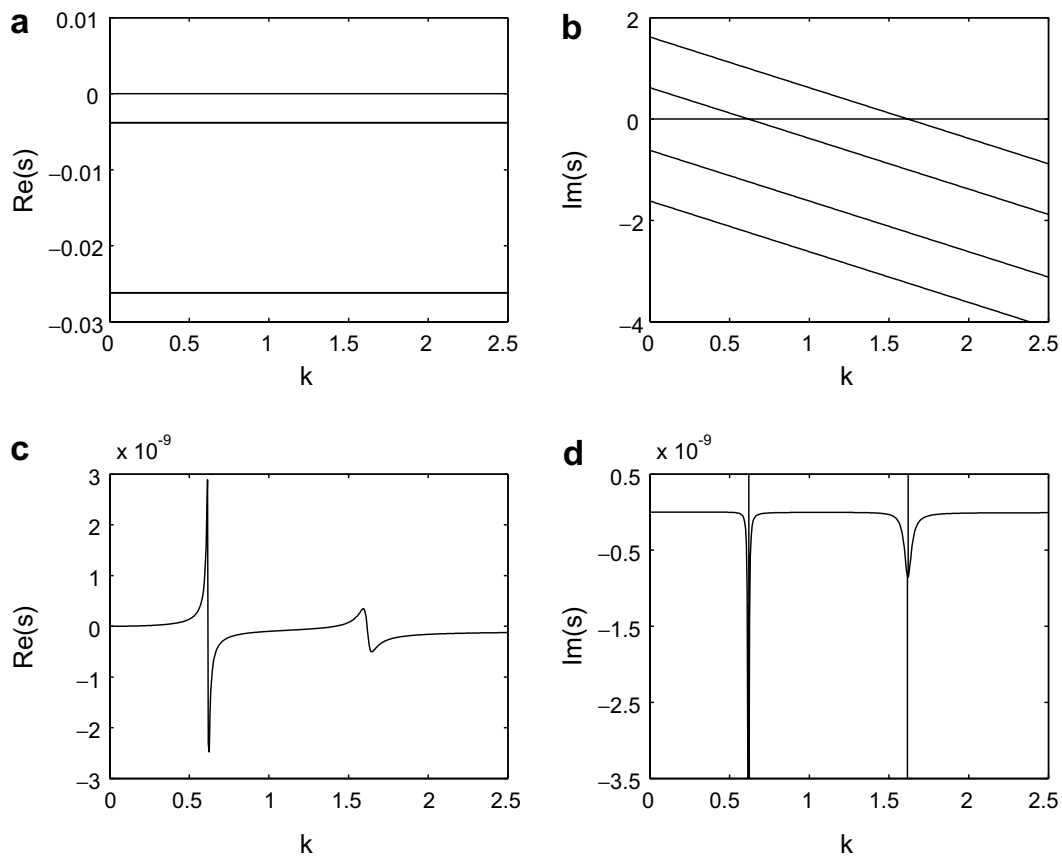


Fig. 8. Two-degree-of-freedom system. Resulting eigenvalues from Eq. (16) for  $m_1 = m_2 = 1$  kg,  $k_1 = k_2 = 1$  N/m,  $d_1 = d_2 = 0.02$  kg s<sup>-1</sup>,  $a_0 = a(H_0) = 10^{-10}$  s kg<sup>-1</sup>,  $V = 1$  m/s,  $\beta = 0.0$  and  $\Gamma = 0.1$ . (a) and (b) show the full range, (c) and (d) give magnified views of the eigenvalues corresponding to surface evolution.

To the knowledge of the authors presently the only contribution to this question seems from Bellette et al. (2006), focussed on the application of rail corrugation. They observed a significant reduction of growth rate with increasing width (in terms of standard deviation) of the relative velocity's distribution function. Taking into account uniform, triangular and normal distributions they argue for deliberately chosen operation strategies to reduce wear-pattern growth. Results on the selection of wavelengths and on the lateral propagation of the patterns have however not been given.

Since the primary motivation for the present work lies in braking systems, where relative sliding speeds depend strongly on driving cycles, an approach to evaluate the effect of distributions of relative sliding speeds on the generation of wear patterns is devised. Although the approach is general in the sense that arbitrary distribution functions could be assumed, the analysis is restricted on the archetypical cases of normal distributions – mimicking a scatter in an otherwise prescribed mean sliding velocity – and uniform distributions with cut-offs at low and at high speeds.

#### 4.1. The linear stability approach

The fundamental idea, as well as also the limitation of the approach chosen, lies in assuming sort of a weighted-averaging approach for the growth of perturbations. Assume that the probability of finding the system with a relative velocity of  $V$  is given by  $p(V)$  and the complex dispersion relation depending on  $V$  and  $k$  is given by  $s(V, k)$ . Then the resulting dispersion relation for perturbations under the probabilistically specified load situation can be calculated as

$$s(k) = \int \frac{p(V)}{V} s(V, k) dV. \tag{18}$$

Basically,  $s(k)$  results from an average over  $s(V, k)$ , weighted with the probability of occurrence for a given  $V$ . In addition a rescaling by a factor  $1/V$  has to be introduced, taking into account that in the present continuum model the number density of passes is proportional to  $V$ . Since the probability of occurrence for a single pass is however already fully included in  $p(V)$ , a corrective factor is necessary.

That the approach sketched is basically a linear extension of the linear stability analysis given before to a statistically defined load case can be seen as follows: for a given specific  $V$  a perturbation grows as  $\exp(s(k)t)$ , which for small  $t$  can be represented by its linear terms  $(1 + s(k)t)$ . Scaling this growth on a unit number density of passes results in  $(1 + \frac{s(k)}{V}t)$ . When different  $V$ s exist in a loading situation, these terms have to be combined in a multiplicative way, such that the resulting perturbation has an amplitude proportional to  $\prod [1 + \frac{s(V,k)t}{V}]^{n(V)}$ , where  $n(V)$  specifies the number of cases in which  $V$  is obtained. For small  $t$  the expression corresponds to  $1 + \sum_V \frac{n(V)s(V,k)t}{V}$ . In the continuum limit this expression directly leads to the weighted average formula given above in Eq. (18).

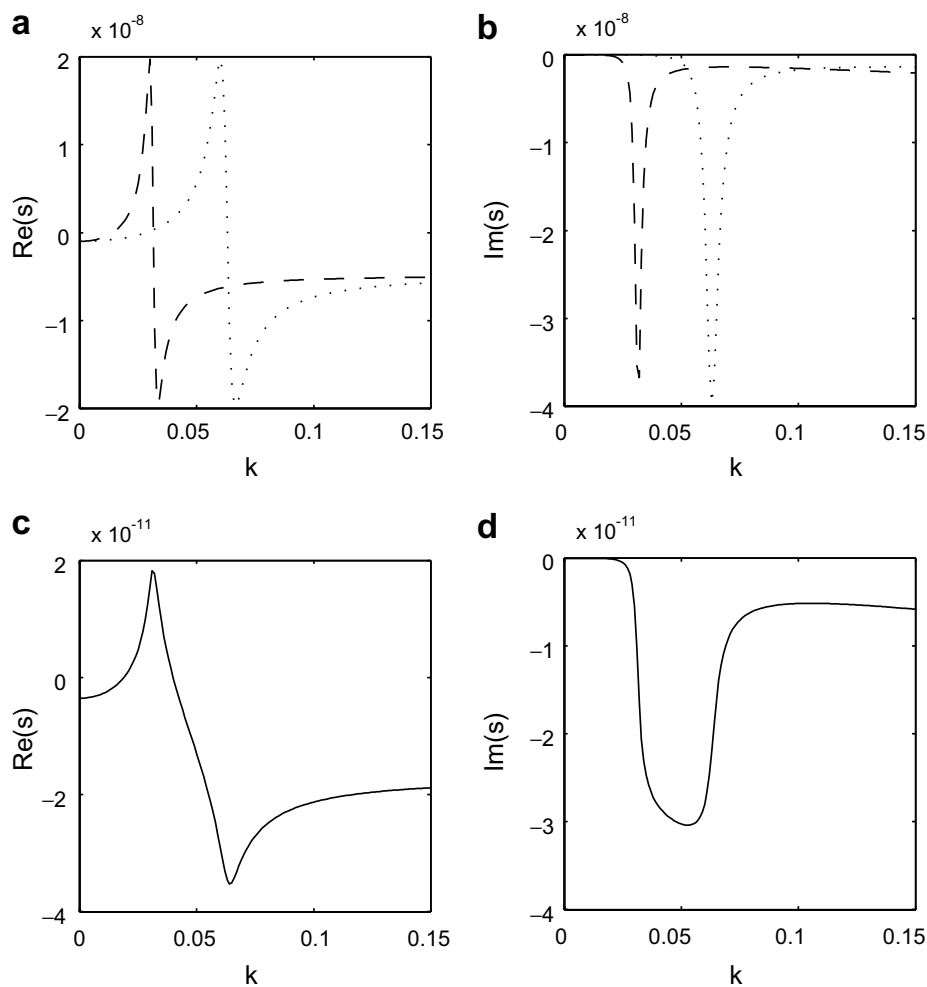


Fig. 9. Results of stability analysis of a system with  $m = 1 \text{ kg}$ ,  $\Gamma = 0.1$ ,  $\omega = 2\pi \text{ s}^{-1}$ ,  $\beta = 1.0 \times 10^{-9} \text{ s}^{-1}$ ,  $a(H_0) = 1.0 \times 10^{-10} \text{ s kg}^{-1}$ , subjected to a uniform distribution of relative velocities  $100 < V < 200$ . (a) and (b) show  $\text{Re}(s)$  and  $\text{Im}(s)$  for fixed  $V = 100$  (dotted) and  $V = 200$  (dashed). (c) and (d) give the resulting growth rates  $\text{Re}(s)$  and frequencies  $\text{Im}(s)$  for the system subjected to the distribution of relative velocities.

#### 4.2. Uniform distributions

First a constant probability density function with a cutoff at a lower and at a higher velocity is considered, Fig. 9. A number of results can be noticed. First, the perturbation of strongest growth corresponds closely to the lowest wavenumber that may be generated through the velocity-band. In addition, the resulting growth rate is strongly reduced. Due to the weighted-averaging approach the phenomenon can easily be understood: only for the lowest wavenumbers the superposition of the individual dispersion relations is mostly constructive. For larger wavenumbers contributions due to other relative velocities  $V$  act in a destructive fashion. The resulting reduction in maximum growth rate is in satisfactory agreement with earlier findings of Bellette et al. (2006), who use a different calculation approach. In addition to Bellette et al. (2006), the present analysis allows however also for an evaluation of the most unstable wavelength and the pattern's drift velocity. It in addition turns out that also the drift velocity is substantially reduced, such that for probabilistically specified  $V$  the emerging patterns should remain rather stationary in space. Again the origin of the effect may be traced back to an interference argument as given above already for the growth rate.

To summarize the results: whenever there is a band of relative velocities with equal probability, patterns seem to emerge that have more or less the smallest wavenumber, or the largest wavelength, that can be attributed to a velocity in the given band; in fact one could think that only the high-velocity contributions yield instability, whereas all velocity contributions corresponding to smaller relative velocities are 'lost' due to destructive interference. Also one should note that the most unstable wavelength is by far not given by the average value of the velocity distribution: in the case of constant  $p(V)$  it is not the mean value, but it is the upper cutoff-velocity that decides on wavelength selection.

#### 4.3. Gaussian distributions

As a second generic load case, normal distributions of  $V$  around a mean value are considered. Also here it turns out that the wavenumber of the most unstable mode does – for significant width of  $p(V)$  – not correspond to the mean velocity, but is shifted towards lower wavenumbers. Fig. 10 gives results for the resulting dispersion relations for  $\sigma/V_0 = 10\%$ ,  $20\%$ ,  $30\%$ . It is clear that the maximum growth rate is reduced for increasing width of the underlying distribution, and that also the wavenumber corresponding to the most strongly growing mode is shifted to smaller values.

Fig. 11 summarizes the findings. The growth rate reduction (also detected already by Bellette et al., 2006), is quite marked whenever the distribution  $p(V)$  gains non-zero width, then decays only moderately. In addition, the wavenumber corresponding to the most unstable mode decreases rather linearly from its value obtained for constant  $V_0$ .

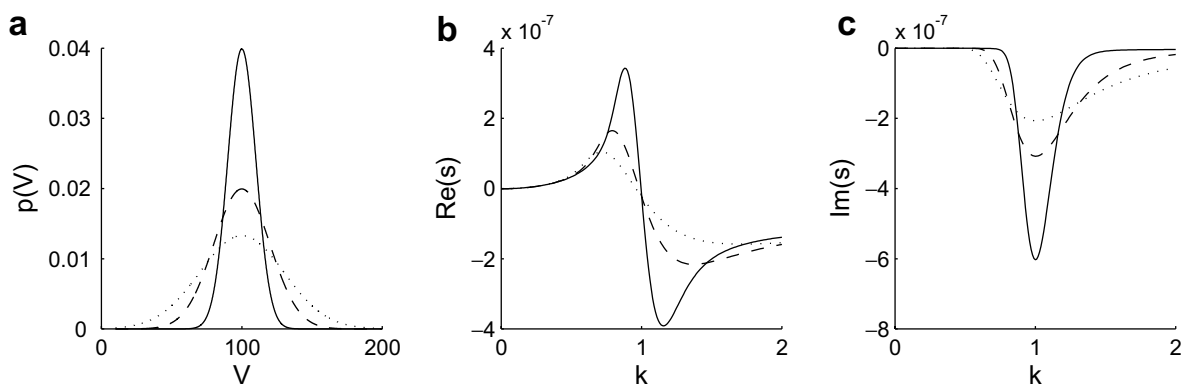


Fig. 10. Results of stability analysis of a system with  $m = 1 \text{ kg}$ ,  $\Gamma = 0.01$ ,  $\omega_0 = 100 \text{ s}^{-1}$ ,  $\beta = 0.5 \times 10^{-8} \text{ s}^{-1}$ ,  $a(H_0) = 1.0 \times 10^{-10} \text{ s kg}^{-1}$ , subjected to Gaussian distributions of relative velocities. (a) shows distribution functions  $p(V)$  centered around  $V_0 = 100$  with standard deviations  $\sigma$  equal to 10 (solid line), 20 (dashed) and 30 (dotted). (b) and (c) give the corresponding real and imaginary parts of the dispersion relation for perturbations subjected to the randomly specified relative velocities.

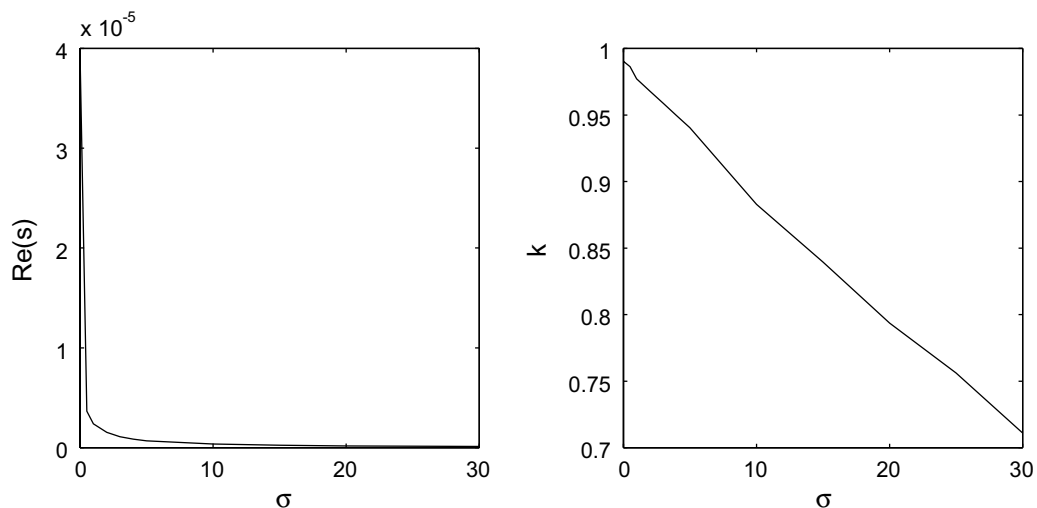


Fig. 11. Maximum growth rate (left) and corresponding wavenumber (right) vs. width  $\sigma$  of the Gaussian velocity distribution for the system used in Fig. 10.

The findings have a number of consequences. Not only, that finite-width velocity distributions reduce the growth, offering a simple approach against pattern emergence. Moreover, the marked curves shown in Fig. 11 suggest that even in situations where  $V$  is typically assumed as constant, one might not be so sure about it, since already small variations around  $V_0$  lead to large reductions in pattern growth. Also: when the relative width of the velocity distribution becomes rather large, the effects due to constructive or destructive interference become so marked, that the most unstable, and hence probably emerging pattern, cannot any more be predicted by the mean velocity  $V_0$ . In our example, for  $\sigma/V_0 = 30\%$ , the wavenumber of the most unstable mode has fallen to around 0.7 times the wavenumber that would have been expected due to the most probable  $V$ . Conclusively, the emerging pattern should have a wavelength much larger than what would have been expected from the mean relative velocity.

At this point it seems sensible to terminate the discussion of the results obtained. Already the two simple probability distributions investigated have shown that non-constant relative velocities generally lead to a reduction of the patterns growth and drift; in addition the resulting wavelengths will turn out larger than what could be expected from simplified calculations taking into account only the relative velocities' mean value. The specifics and quantitative features of the effect do however seem to depend strongly on the specifics of the underlying distribution function, which therefore needs to be known to obtain satisfactory results on growth and drift rates, as well as on the emerging wavelength.

## 5. Summary, conclusions and outlook

The present work shows how structural resonances from a linear structural system in sliding motion are related to instabilities in the surface evolution due to wear. Using simple minimal models a number of results have been obtained: (1) For constant relative velocities linear instabilities of the surface evolution, i.e. eigenmodes of the linearized surface evolution equation with corresponding eigenvalues having positive growth rates, always appear close to those surface wavenumbers which correspond to structural resonances. (2) For weakly damped systems instability results only in wavenumber-intervals close to the corresponding structural resonance frequencies. For strongly damped systems also wavenumbers much larger than the resonance-related one may belong to unstable modes. (3) In the single-degree-of-freedom system physically the instability can be traced back to the structural oscillation in phase with the perturbation of the topography. Out-of-phase oscillation components, as they arise in damped systems when the structural resonance frequency is approached, lead to non-zero imaginary parts in the eigenvalues of the linearized surface evolution equation, which means that the generated surface-topography waves are not stationary in space but slowly move laterally. (4) Multi-degree-of-freedom systems generally behave similar to single-degree-of-freedom systems. (5) An

averaging approach for both single- and multi-degree-of-freedom systems has been presented and discussed that allows the determination of the surface evolution after elimination of the structural degrees of freedom. (5) When the relative velocities are given only in statistical terms, e.g. due to load cases where different relative velocities may appear, growth or decay of surface perturbations is given by a linear superposition of the results for constant relative velocities. This generally results in (a) a decrease of the growth rate of the most unstable mode, (b) a decrease of the wavenumber of the most unstable mode (when the system is weakly damped), and (c) a decrease of the perturbations' propagation speed for all modes. All effects are substantial, when the underlying distribution functions are non-trivial.

Among the points still to be addressed in future studies, one may find:

- *Extended contact area.* Most relevant technical contacts have a finite extension. When structural oscillations come into play, they will typically be accompanied by a distributed oscillatory contact pressure distribution. This behavior is not yet captured in the point-contact model considered.
- *Finite-size wear regions.* In a number of technically relevant systems the surface subjected to wear is not infinite in spatial extent, but finite: e.g. in friction brakes the brake disk is characterized by a finite circumferential length. It is obvious that the present analysis for infinitely extended systems can easily be extended to such finite-size systems by constraining the allowable wavenumbers to the discrete set of values corresponding to the underlying periodic boundary conditions.
- *Structural nonlinearities.* The role of nonlinearities in the structural system has not yet been investigated in the present context. This might however often be relevant, since due to the typically strong normal preload materials in contact often show at least nonlinear stiffness characteristics.
- *Nonlinear surface-topography evolution.* The approaches presented are basically linearized stability analyses; i.e. exponentially growing unstable modes are determined. Questions with respect to amplitude saturation, or finite-amplitude issues, are not yet addressed. For growing surface corrugation such finite-amplitude effects might however become more important.

It is obvious that the present approach to modeling and simulating wear pattern generation has still to prove its feasibility, especially when it comes to use in practical engineering environments. However, when comparing the presented 'frequency-domain' type of approach to direct computations of the coupled vibration and wear phenomena, it seems that the stability analysis contributes well to both understanding as well as to computability of wear-pattern generation. On the other hand side, its limitations due to the underlying linearization procedures are also obvious. Overall, the task to develop useable modeling and simulation procedures for the problem at hand will require further investigation.

## References

- Afferante, L., Ciavarella, M., Barber, J.R., 2006. Sliding thermoelastodynamic instability. *Proceedings of the Royal Society A* 24, 3895–3904.
- Bellette, P.A., Meehan, P.A., Daniel, W.J.T., 2006. Investigation into the effect of speed variation on the growth of wear-type rail corrugation. In: *Proceedings of the First Australasian Acoustical Societies Conference*, pp. 227–234.
- Bhaskar, A., Johnson, K.L., Wood, G.D., Woodhouse, J., 1997. Wheel-rail dynamics with closely conformal contact. Part 1. Dynamic modeling and stability analysis. *Proc. Inst. Mech. Eng.* 211 (F), 11–26.
- Both, J.A., Hong, D.C., Kurtze, D.A., 2001. Corrugation of roads. *Physica A* 301, 545–559.
- Brommundt, E., 1997. A simple mechanism for the polygonalization of railway wheels by wear. *Mech. Res. Commun.* 24, 435–442.
- Charru, F., Hinch, E.J., 2006. Ripple formation on a particle bed sheared by a viscous liquid. Part 1. Steady flow. *J. Fluid Mech.* 550, 111–121.
- Frischmuth, K., Langemann, D., 2003. Distributed numerical calculations of wear in the wheel-rail contact. In: Popp, K., Schiehlen, W. (Eds.), *System Dynamics and Long-Term Behaviour of Railway Vehicles, Track and Subgrade*. Springer-Verlag, Berlin, pp. 85–100.
- Grassie, S.L., Edwards, J.W., 2006. Development of Corrugation as a result of varying normal load. In: *7th International Conference on Contact Mechanics and Wear of Rail/Wheel Systems*, Brisbane, Australia.
- Grassie, S.L., Kalousek, J., 1993. Rail corrugation: characteristics, causes and treatments. *J. Rail Rapid Transit, Proc. Inst. Mech. Eng.* 207F, 57–68.
- Küsel, M., Brommundt, E., 2003. Wavy Wear Pattern on the Tread of Railway Wheels. In: Popp, K., Schiehlen, W. (Eds.), *System Dynamics and Long-Term Behaviour of Railway Vehicles, Track and Subgrade*. Springer-Verlag, Berlin, pp. 2121–2132.
- Kurtze, D.A., Hong, D.C., Both, J.A., 2001. The genesis of washboard roads. *Int. J. Mod. Phys. B* 15, 3344–3346.

- Meehan, P.A., Daniel, W.J.T., Campey, T., 2005. Prediction of the growth of wear-type rail corrugation. *Wear* 258, 1001–1013.
- Meehan, P.A., Daniel, W.J.T., 2006. Effects of wheel passing frequency on wear-type corrugations. In: 7th International Conference on Contact Mechanics and Wear of Rail/Wheel Systems, Brisbane, Australia.
- Meinders, T., Meinke, P., 2003. Rotor Dynamics and Irregular Wear of Elastic Wheelsets. In: Popp, K., Schiehlen, W. (Eds.), *System Dynamics and Long-Term Behaviour of Railway Vehicles, Track and Subgrade*. Springer-Verlag, Berlin, pp. 133–152.
- Meywerk, M., Brommundt, E., 1997. Ein phänomenologisches Verschleissmodell für ein Rad-Schiene-System. *Zeitschrift für angewandte Mathematik und Mechanik* 77, 3895–3904.
- Meywerk, M., Brommundt, E., 2000. Evolution of wear patterns on railway wheels. *Zeitschrift für angewandte Mathematik und Mechanik* 80, S355–S356.
- Müller, S., 2001. A linear wheel-rail model to investigate stability and corrugation on straight track. *Wear* 249, 1117–1127.
- Nielsen, J.C.O., Lunden, R., Johansson, A., Verneresson, T., 2003. Train-track interaction and mechanisms of irregular wear on wheel and rail surfaces. *Vehicle Syst. Dyn.* 40, 3–54.
- Sato, Y., Matsumoto, A., Knothe, K., 2002. Review on rail corrugation studies. *Wear* 253, 130–139.
- Schumann, M., Winner, H., 2006. Analyseverfahren zur Beurteilung des ungleichförmigen Bremsscheibenverschleisses an PKW-Scheibenbremsen. In: XXVI Internationales  $\mu$ -Symposium. Berlin, pp. 35–67.
- Steffen, T., 1998. Untersuchung der Hotspotbildung bei Pkw-Bremsscheiben. VDI Fortschritt-Berichte, Reihe 12, Nr. 345. VDI-Verlag, Düsseldorf.